


 Cite this: *RSC Adv.*, 2020, 10, 29536

# A near-infrared fluorescent probe with an improved Stokes shift achieved by tuning the donor–acceptor–donor character of the rhodamine skeleton and its applications†

 Jin Gong,<sup>ab</sup> Chang Liu,<sup>a</sup> Xiaojie Jiao,<sup>a</sup> Song He,<sup>a</sup> Liancheng Zhao<sup>ab</sup> and Xianshun Zeng<sup>id</sup>\*<sup>ab</sup>

In this paper, we report a novel near-infrared (NIR) mitochondrion-targeted fluorescent probe, **RQS**, with an improved Stokes shift (96 nm) for the specific detection of mitochondrial mercury ion ( $\text{Hg}^{2+}$ ) because mitochondrion is one of the main targeted organelles of  $\text{Hg}^{2+}$ . For the preparation of the probe, a novel asymmetrical fluorescent xanthene dye **RQ** was first synthesized by tuning the donor–acceptor–donor (D–A–D) character of the rhodamine skeleton, and then the probe **RQS** was constructed by the mechanism of mercury-promoted ring-opening reaction. As expected, **RQS** could be used for the specific detection of  $\text{Hg}^{2+}$  with high selectivity, high sensitivity, and a detection limit down to the nanomolar range (2 nM). Importantly, **RQS** is capable of specifically distributing in mitochondria, and thus detect  $\text{Hg}^{2+}$  in real-time and provided a potential tool for studying the cytotoxic mechanisms of  $\text{Hg}^{2+}$ .

 Received 16th May 2020  
 Accepted 23rd July 2020

DOI: 10.1039/d0ra04373g

[rsc.li/rsc-advances](http://rsc.li/rsc-advances)

## Introduction

Heavy metal pollution has received increasing attention because it can not only cause serious damage to the environment, but also cause extremely serious injuries to the human body.<sup>1</sup> Mercury ion ( $\text{Hg}^{2+}$ ) is the most representative toxic metal of the numerous heavy metal ions, which is consumed directly and *via* the aggregation of the food chain.<sup>2</sup> It has been reported that mitochondrion is one of the main targeted organelles of  $\text{Hg}^{2+}$ ,<sup>3</sup> that causes serious physiological problems such as nervous system damage and cognitive disorder by denaturing proteins and inactivating enzymes.<sup>4</sup> To date, although a large number of studies have been carried out by researchers,<sup>5</sup> the mechanism of mitochondrial toxicity induced by  $\text{Hg}^{2+}$  has not been fully elucidated. It has been argued that the mitochondrial toxicity of  $\text{Hg}^{2+}$  is caused by its influence on the fluidity and permeability of the membrane, and the damage of the inner mitochondrial membrane is observed by transmission electron microscopy.<sup>5a,d</sup> However, transmission electron microscopy is not suitable for analyses in living cells.<sup>5d</sup> Therefore, the development of mitochondrion-targeted detection tools has practical significance for revealing the cytotoxic mechanism of  $\text{Hg}^{2+}$  in living cells.

In recent years, the fluorescent probe imaging technology has been introduced for the detection of  $\text{Hg}^{2+}$  due to its high sensitivity, high selectivity, and non-invasive and real-time detection.<sup>6</sup> In particular, derivatives of rhodamine have been widely designed and synthesized for the detection of  $\text{Hg}^{2+}$  due to their excellent water solubility, high quantum efficiency, high photo-stability, excellent water solubility and distinct photo-physical advantages of the ring-opening process.<sup>7</sup> Upon the specific spirolactam-opening process, the non-fluorescent spirocyclic forms of rhodamine-based probes were converted irreversibly to the ring-opened high fluorescent species, resulting in highly sensitive “*turn-on*” detection of  $\text{Hg}^{2+}$ .<sup>7b,f</sup> However, most of the reported rhodamine-based  $\text{Hg}^{2+}$  probes bear some drawbacks, for example, short emission wavelength (<600 nm) and narrow Stokes shifts (<30 nm), which limit their biological imaging applications.<sup>8</sup> The development of probes capable of detecting  $\text{Hg}^{2+}$  in the near-infrared (NIR) region (>650 nm) is particularly important for imaging applications because it can avoid auto-fluorescence interference of biological backgrounds and reduce photo-damage to living samples.<sup>9</sup> At the same time, fluorescent probes with large Stokes shifts can avoid self-quenching, excitation wavelength interference and poor signal-to-noise ratio, resulting in precise imaging and accurate sensing.<sup>10</sup> In addition, number of  $\text{Hg}^{2+}$  probes suffer from high detection limit, slow response time and poor membrane permeability hampering their application in biological systems. Unfortunately, up to now, mitochondrion-targeting NIR fluorescent probes of rhodamine derivatives with large Stokes shifts were rarely described for the specific detection of  $\text{Hg}^{2+}$ .<sup>6c</sup> Consequently, it is of great significance to develop new mitochondrion-targeted NIR fluorescent probes

<sup>a</sup>Tianjin Key Laboratory for Photoelectric Materials and Devices, School of Materials Science & Engineering, Tianjin University of Technology, Tianjin, 300384, China. E-mail: xshzeng@tjut.edu.cn

<sup>b</sup>School of Materials Science and Engineering, Harbin Institute of Technology, Harbin, 150001, China

† Electronic supplementary information (ESI) available. See DOI: 10.1039/d0ra04373g



based on rhodamine scaffolds with large Stokes shifts, for sensing of  $\text{Hg}^{2+}$  at a subcellular level.

Changing the intramolecular charge transfer (ICT) properties of the  $\pi$ -conjugate, e.g. fine tuning the donor-acceptor-donor (D-A-D) character of the chromophore by changing the position of electron-donating groups on the chromophoric skeleton, is shown to be an efficient strategy to increase both the Stokes shifts and emission wavelengths.<sup>11</sup> In 2013, Zhang and coworkers demonstrated that the emission wavelengths of rhodamine dyes are prominently red-shifted by using a 1,4-diethyl-1,2,3,4-tetrahydroquinoxaline unit as a strong electron-donating group to modify the xanthene moiety, increased with the Stokes shifts.<sup>12</sup> In the past few years, we found that when the molecules were in an asymmetrical state, the Stokes shifts of them were largely increased (Scheme 1).<sup>11,13</sup> These phenomena encouraged and inspired us to design probes with longer emission wavelengths and larger Stokes shifts by tuning the D-A-D character of rhodamine dyes. In addition, the cationic xanthene moiety normally works as a functional group for targeting mitochondria and increases the water solubility of the probe.<sup>14</sup> Herein, a novel xanthene dye **RQ** with an NIR emission wavelength and a large Stokes shift was first prepared by introducing an electron-donating 1,4-diethylpiperazine moiety into the rhodamine scaffold, and then the probe **RQS** was constructed by the mechanism of well-known mercury-promoted ring-opening reaction.<sup>15</sup> As expected, **RQS** is an outstanding “turn-on” fluorescent probe, and it can be used for the specific detection of  $\text{Hg}^{2+}$ . Importantly, **RQS** is capable of specifically distributing in the mitochondria, and thus detect  $\text{Hg}^{2+}$  in real-time there, which provided a potential tool for studying the cytotoxic mechanisms of  $\text{Hg}^{2+}$ . In the case of scarcity of NIR probes with large Stokes shifts for monitoring  $\text{Hg}^{2+}$  in mitochondria, this work is of great importance.

## Results and discussion

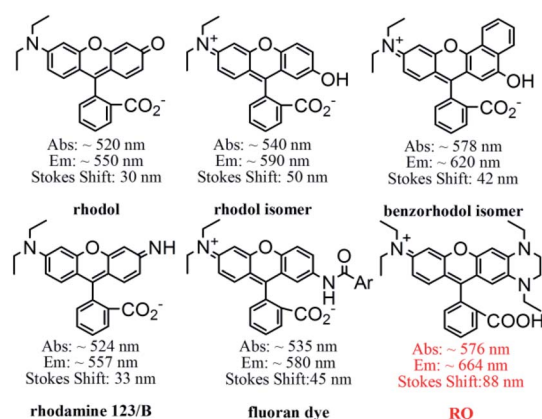
### Molecular synthesis

The synthetic procedures and methods for the dye **RQ** and the probe **RQS** are described in Scheme 2. The intermediate

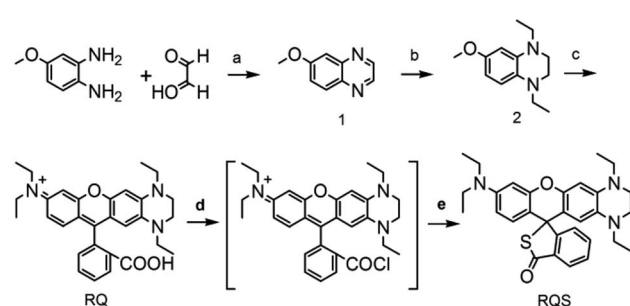
compounds 4-methoxy-1,2-phenylenediamine (**1**) and 1,4-diethyl-6-methoxy-1,2,3,4-tetrahydroquinoxaline (**2**) were synthesized according to the literature.<sup>12,15d</sup> By the reaction of 2-(4-diethylamino-2-hydroxybenzoyl)benzoic acid with **2**, the dye **RQ** was obtained in 76% yield. With the reaction of **RQ** and oxalyl chloride in dry dichloromethane, followed by the treatment with excess  $\text{Na}_2\text{S}$  saturated aqueous solution, the probe **RQS** was produced in 62% yield. The structures of the new compounds **RQ** and **RQS** were characterized by spectroscopic techniques, for example,  $^1\text{H}$  NMR,  $^{13}\text{C}$  NMR and HRMS, and the spectra are presented in the ESI (Fig. S1–S6†).

### Characterization of RQ

In order to verify whether **RQ** meets our original design intentions, a detailed evaluation of the photophysical properties of the dye **RQ** in distinct solvents ( $\text{CH}_3\text{CN}$ , DCM, DMSO, EtOH, and  $\text{H}_2\text{O}$ ) was conducted. Surprisingly, the dye **RQ** showed the maxima absorption bands between 573 nm and 582 nm, and the maxima emission peaks of **RQ** range from 661 nm to 670 nm in all test solvents (Table S1 and Fig. S7†). **RQ** showed strong absorption but weak fluorescence in  $\text{H}_2\text{O}$ , which might be due to the hydrogen-bonding interaction between water and dye molecules. Comparatively, **RQ** showed longer emission and a larger Stokes shift than traditional rhodamine dyes in ethanol (Table 1). The maximum fluorescence emission of the dye was remarkably red-shifted *ca.* 70 nm (rhodamine 101), 95 nm (rhodamine B), and 109 nm (rhodamine 6G) respectively, which may be attributed to the excited intramolecular charge transfer (ICT). Meanwhile, the Stokes shift of **RQ** was 88 nm in ethanol, which was significantly larger than rhodamine 101 (30 nm), rhodamine B (26 nm), and rhodamine 6G (28 nm). Importantly, the asymmetric dye **RQ** exhibited a longer emission wavelength and a larger Stokes shift than the dye Rh Q-H with a symmetric structure (Table 1).<sup>11</sup> It can be rationalized that the change of the electron-donating 1,4-diethylpiperazine group in the asymmetric xanthene fluorophore can regulate the donor-acceptor-donor (D-A-D) character of the chromophore. The donor-acceptor system in plane from the electron-donating 1,4-diethylpiperazine group to the electron-withdrawing group in **RQ** can



Scheme 1 Emission wavelength span, structures and absorption/emission data of examples of asymmetrical compounds and **RQ**.



Scheme 2 Synthesis of **RQ** and **RQS**. Reagents and conditions: (a)  $\text{CH}_3\text{CN}$ , 60 °C, 6 h; (b)  $\text{NaBH}_4$ ,  $\text{CH}_3\text{CO}_2\text{H}$ , dry toluene, 5 °C to reflux, 5 h; (c) 2-(4-diethylamino-2-hydroxybenzoyl)benzoic acid, methanesulfonic acid, 80 °C, overnight, 76%; (d) oxalyl chloride, dry dichloromethane, room temperature, 4 h; (e) saturated  $\text{Na}_2\text{S}$  aqueous solution, room temperature, 10 h, 62%.



**Table 1**  $\lambda_{\text{abs}}$  and  $\lambda_{\text{em}}$  values of RQ, rhodamine 101, rhodamine B, rhodamine 6G and Rh Q–H in EtOH<sup>11</sup>

Dyes	$\lambda_{\text{abs}}$ (nm)	$\lambda_{\text{em}}$ (nm)	$\Delta\lambda$ (nm)
Rhodamine 101	564	594	30
Rhodamine B	543	569	26
Rhodamine 6G	527	555	28
Rh Q–H	597	644	47
<b>RQ</b>	576	664	88

lead to large changes in the energy difference between the ground and the excited state, thereby producing an obviously increased Stokes shift.<sup>16</sup> Furthermore, the quantum yields of RQ range from 7% to 33% in these solvents (Table S1<sup>†</sup>). Collectively, it proved that RQ is a novel NIR fluorescent reagent with a large Stokes shift, achieving original design intentions.

### Fluorescence imaging of RQ in HeLa cells

The excellent optical properties, for example, NIR emission wavelength and improved Stokes shifts, encouraged us to evaluate the potential applications of RQ in living cells. As shown in Fig. S8,<sup>†</sup> the standard MTT assay confirmed that the dye RQ has extremely low cytotoxicity. Then, imaging experiments of RQ were conducted in living cells. After treatment with RQ (0.1  $\mu\text{M}$ ) for 30 minutes, a strong red fluorescence signal was observed, as shown in Fig. S9,<sup>†</sup> indicating that RQ is membrane permeable and can be used as an imaging reagent in living cells. Meanwhile, RQ tended to accumulate in one of the organelles. In order to investigate the localization characteristics of RQ, co-localization experiments were carried out using commercial targeting reagents Mito-Tracker Green (Mito), ER-Tracker Green (ER), Lyso-Tracker Green (Lyso), and Golgi-Tracker Green (Golgi). As shown in Fig. 1a, highlighted yellow pixels were observed on the overlapping image, and a high overlap coefficient (0.93) and Pearson's coefficient (0.93) could be calculated from the intensity correlation plot, suggesting that RQ was mainly accumulated in the mitochondria. In contrast, red fluorescence signals of RQ and green fluorescence signals of other targeting reagents (Lyso, ER, and Golgi) were obviously distributed in different organelles (Fig. 1b–d), and low overlap coefficients and Pearson's coefficients were also observed. Collectively, RQ is membrane permeable and can be used as an effective mitochondrion-targeting reagent.

### Recognition properties of RQS

Since RQ possessed the unique spirocyclic/open-ring process of rhodamines that could be used as an effective platform in constructing fluorescent turn-on sensors, RQS was constructed by the well-known  $\text{Hg}^{2+}$ -promoted ring-opening reaction.<sup>15</sup> In order to assess the sensitivity of RQS towards  $\text{Hg}^{2+}$ , we conducted continuous titration experiments by fluorescence spectroscopy. As shown in Fig. 2, upon addition of increasing concentrations of  $\text{Hg}^{2+}$  (0–2.0 equiv.) to the solution, the emission intensity gradually increased, and eventually reached

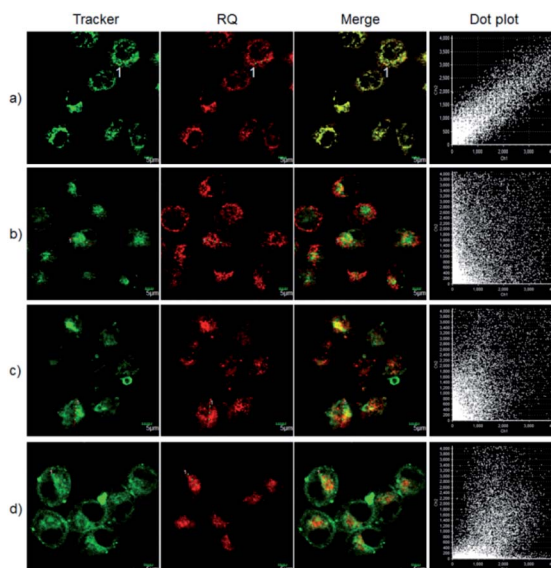


**Fig. 1** Co-localization experiments with HeLa cells stained with RQ (0.1  $\mu\text{M}$ ) and 200 nM targeting reagents (Lyso-Tracker Green (Lyso), Mito-Tracker Green (Mito), ER-Tracker Green (ER), and Golgi-Tracker Green (Golgi)): (a) costained with Mito; (b) costained with Lyso; (c) costained with Golgi; and (d) costained with ER. Red channel:  $\lambda_{\text{ex}} = 559 \text{ nm}$ ,  $\lambda_{\text{em}} = 520\text{--}541 \text{ nm}$ ; green channel:  $\lambda_{\text{ex}} = 488 \text{ nm}$ ,  $\lambda_{\text{em}} = 618\text{--}718 \text{ nm}$ .

the plateau when the amount of  $\text{Hg}^{2+}$  reached 2 equivalent. The emission intensity at 680 nm increased more than 87 times, and the linear fitting could be obtained between  $\text{Hg}^{2+}$  concentrations ranging from 0 to 16  $\mu\text{M}$  and the emission intensity at 680 nm. Then, the detection limit of  $\text{Hg}^{2+}$  was obtained to be 2 nM based on the equation of  $3\sigma/k$ , where  $k$  is the slope plotted from the fluorescence intensity at 680 nm versus the concentration of  $\text{Hg}^{2+}$ , and  $\sigma$  is the relative standard deviation of 10 times fluorescence measurements of the blank solution in parallel. Compared with reported probes, the detection limit of RQS is at a low level, and the detailed data are listed in Table S2<sup>†</sup>. Simultaneously, the detection limit is far lower than the U.S. EPA's (Environmental Protection Agency) limit on drinking water (9.97 nM),<sup>17</sup> suggesting that RQS could be used as a practical probe for the quantitative detection of  $\text{Hg}^{2+}$  in an aqueous environment.

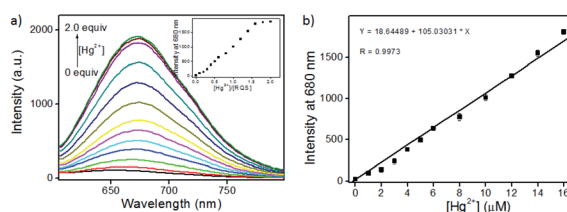


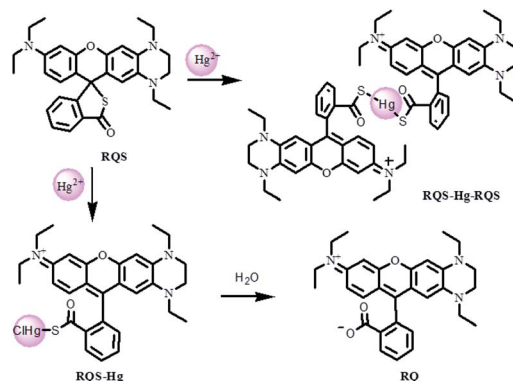
**Fig. 2** (a) Fluorescence changes of RQS (10  $\mu\text{M}$ ) treated with increasing concentrations of  $\text{Hg}^{2+}$  (0–2.0  $\mu\text{M}$ ). Inset: the plot of the fluorescence intensities at 680 nm versus the equivalents of  $\text{Hg}^{2+}$  and (b) the plot of the fluorescence intensities of RQS at 680 nm versus the concentrations of  $\text{Hg}^{2+}$  (0–16  $\mu\text{M}$ ). The conditions: HEPES buffer (10 mM, pH 7.4),  $\lambda_{\text{ex}} = 585 \text{ nm}$ , slit = 10/10 nm.





Selectivity is also an important indicator of probe recognition ability, hence we then performed selective experiments by utilizing distinct metal ions that are generally available in surface water, such as  $\text{Ag}^+$ ,  $\text{Al}^{3+}$ ,  $\text{Ca}^{2+}$ ,  $\text{Cd}^{2+}$ ,  $\text{Co}^{2+}$ ,  $\text{Cr}^{3+}$ ,  $\text{Cu}^{2+}$ ,  $\text{Fe}^{2+}$ ,  $\text{Fe}^{3+}$ ,  $\text{Hg}^{2+}$ ,  $\text{K}^+$ ,  $\text{Li}^+$ ,  $\text{Mg}^{2+}$ ,  $\text{Mn}^{2+}$ ,  $\text{Na}^+$ ,  $\text{Ni}^{2+}$ ,  $\text{Pb}^{2+}$ ,  $\text{Pd}^{2+}$ , and  $\text{Zn}^{2+}$ . As shown in Fig. 3a and b, upon addition of different metal ions mentioned above, barring  $\text{Hg}^{2+}$ , all other metal ions failed to induce significant changes in the absorption and emission spectra of **RQS**. For  $\text{Hg}^{2+}$ , **RQS** rapidly showed a strong absorption band at 584 nm and a new enhanced emission band at 680 nm was observed, which could be attributed to the formation of a large  $\pi$ - $\pi$  conjugated system through the  $\text{Hg}^{2+}$ -promoted ring-opening reaction.<sup>15</sup> Meanwhile, along with the spectral changes, the solution exhibited an obvious color change from colorless to blue in the presence of  $\text{Hg}^{2+}$  (Fig. S9†), which could be easily monitored by the naked eye. In contrast, insignificant changes in color were observed in the presence of other metal ions. The results revealed that **RQS** can function as a highly selective fluorescent probe for  $\text{Hg}^{2+}$ .

Subsequently, to verify the reaction mechanism, HRMS was carried out to analyze the molecular weight of the probe after the treatment with  $\text{Hg}^{2+}$ . As shown in Fig. S11,† an intense peak at  $m/z$  600.2150 corresponding to  $[\text{RQS} + \text{Hg} + \text{RQS}]^{2+}$  was observed, revealing that the open-ring process was triggered and the complex **RQS-Hg-RQS** was constructed between **RQS** and  $\text{Hg}^{2+}$  (Scheme 3). In addition, the stoichiometry between  $\text{Hg}^{2+}$  and **RQS** was confirmed by a Job's plot analysis, and the concentration ratio revealed a 2 : 1 stoichiometric ratio between **RQS** and  $\text{Hg}^{2+}$  (Fig. 3c). Meanwhile, a mass peak at  $m/z$  734.1644 corresponding to  $[\text{RQS} + \text{HgCl}]^+$  was clearly observed, and then the complex **RQS-Hg** can be further hydrolyzed to **RQ** ( $m/z$  484.2600). In order to further evaluate the selectivity of **RQS** in



Scheme 3 Proposed reaction mode between **RQS** and  $\text{Hg}^{2+}$ .

the presence of interfering metal cations, competition experiments were conducted. The responses of **RQS** toward  $\text{Hg}^{2+}$  in the presence of coexistent potentially interfering metal ions ( $\text{Ag}^+$ ,  $\text{Al}^{3+}$ ,  $\text{Ca}^{2+}$ ,  $\text{Cd}^{2+}$ ,  $\text{Co}^{2+}$ ,  $\text{Cr}^{3+}$ ,  $\text{Cu}^{2+}$ ,  $\text{Fe}^{2+}$ ,  $\text{Fe}^{3+}$ ,  $\text{K}^+$ ,  $\text{Li}^+$ ,  $\text{Mg}^{2+}$ ,  $\text{Mn}^{2+}$ ,  $\text{Na}^+$ ,  $\text{Ni}^{2+}$ ,  $\text{Pb}^{2+}$ ,  $\text{Pd}^{2+}$ , and  $\text{Zn}^{2+}$ ) were tested and recorded under the same conditions. As shown in Fig. 3d, the results of competition experiments revealed that the emission spectral change observed for **RQS** on binding to  $\text{Hg}^{2+}$  remained minor, or no interference was observed in the presence of all other metal ions, confirming the specificity of **RQS** toward  $\text{Hg}^{2+}$ .

In order to evaluate whether **RQS** was suitable for detecting  $\text{Hg}^{2+}$  in a physiological environment, the emission spectra of **RQS** at different pH values were recorded. The pH-dependent fluorescence responses of **RQS** in the absence and presence of  $\text{Hg}^{2+}$  are presented in Fig. S12.† In the absence of  $\text{Hg}^{2+}$ , **RQS** exhibited almost no obvious change in the fluorescence intensity at 680 nm in the pH range of 4.0–10.0, suggesting that the probe is stable in a wide pH region. However, in the presence of  $\text{Hg}^{2+}$ , the fluorescence intensity at 680 nm was obviously enhanced in the pH range of 4.0–9.0 for the formation of a large  $\pi$ -conjugated system, implying that **RQS** could be used to detect  $\text{Hg}^{2+}$  under physiological conditions. At the same time, time-dependent fluorescence responses of **RQS** in the absence and presence of  $\text{Hg}^{2+}$  were analyzed at room temperature to evaluate whether the probe can be used to monitor  $\text{Hg}^{2+}$  in real time. The spectral data were recorded within 300 s after the addition of  $\text{Hg}^{2+}$ . As shown in Fig. S13,† in the absence of  $\text{Hg}^{2+}$ , the emission intensity of **RQS** at 680 nm remained substantially constant, suggesting that **RQS** owned high photo-stability. In contrast, upon addition of 10 equiv. of  $\text{Hg}^{2+}$ , the emission intensity of **RQS** at 680 nm rapidly increased and reached a plateau within about 100 s, implying that **RQS** can be used as an effective candidate for monitoring  $\text{Hg}^{2+}$  in real time. The above-mentioned results indicated that **RQS** was able to sense trace amounts of  $\text{Hg}^{2+}$  in real time in physiological environments.

### Fluorescence imaging of **RQS** in HeLa cells

The excellent spectral properties, for example, high selectivity, high sensitivity, and fast response time, encouraged us to assess the potential applications of **RQS** for imaging  $\text{Hg}^{2+}$  in living

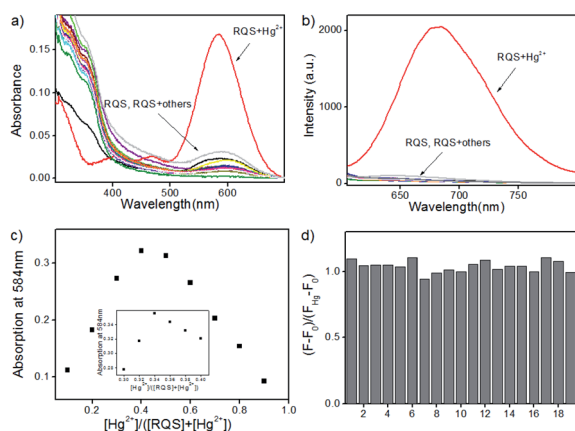


Fig. 3 (a) Absorption and (b) fluorescence emission responses of **RQS** (10  $\mu\text{M}$ ) upon addition of different species; (c) Job's plot of **RQS** and  $\text{Hg}^{2+}$  in HEPES. The total concentration of **RQS** and  $\text{Hg}^{2+}$  was kept fixed at 30  $\mu\text{M}$ . (d) Fluorescence ratio ( $(F - F_0)/(F_{\text{Hg}} - F_0)$ ) changes of **RQS** in the presence of 20  $\mu\text{M}$   $\text{Hg}^{2+}$  and different species. Metal cations (20  $\mu\text{M}$ ): (1)  $\text{Ag}^+$ ; (2)  $\text{Al}^{3+}$ ; (3)  $\text{Ca}^{2+}$  (10 mM); (4)  $\text{Cd}^{2+}$ ; (5)  $\text{Co}^{2+}$ ; (6)  $\text{Cl}^{3+}$ ; (7)  $\text{Cu}^{2+}$ ; (8)  $\text{Fe}^{2+}$ ; (9)  $\text{Fe}^{3+}$ ; (10)  $\text{Hg}^{2+}$ ; (11)  $\text{K}^+$  (10 mM); (12)  $\text{Li}^+$  (10 mM); (13)  $\text{Mg}^{2+}$  (10 mM); (14)  $\text{Mn}^{2+}$ ; (15)  $\text{Na}^+$ ; (16)  $\text{Ni}^{2+}$ ; (17)  $\text{Pb}^{2+}$ ; (18)  $\text{Pd}^{2+}$ ; and (19)  $\text{Zn}^{2+}$ . Conditions: HEPES buffer (10 mM, pH = 7.4),  $\lambda_{\text{ex}}$  = 585 nm, slit = 10/10 nm.



cells. To examine the feasibility of using **RQS** as an imaging reagent to map the cellular uptake of  $\text{Hg}^{2+}$ , the cytotoxicity of the probe to HeLa cells was assessed by the well-established MTT assay. HeLa cells were treated with different concentrations of **RQS** (0, 1, 3, 5, 10, and 20  $\mu\text{M}$ ) for 24 h, 48 h and 72 h, respectively. As shown in Fig. S14,<sup>†</sup> more than 70% of cells survived, suggesting extremely low cytotoxicity of **RQS**, and thus, **RQS** is suitable as an imaging reagent. Subsequently, imaging experiments of **RQS** for monitoring  $\text{Hg}^{2+}$  in living cells were conducted. HeLa cells were incubated with **RQS** (0.1  $\mu\text{M}$ ) for 30 min and then washed with PBS for removing excess and surface-adhered reagents. As shown in Fig. 4a, weak red fluorescence signals in the red channel were observed, revealing the extremely low background of **RQS**. In contrast, an obvious enhancement in red fluorescence signals was observed after treatment with  $\text{Hg}^{2+}$  (0.5  $\mu\text{M}$ ) for 30 min (Fig. 4b). Compared with the controlled cells, the relative enhancement of fluorescence signals is about 75-fold (Fig. 4c). The results indicated that **RQS** was membrane permeable and could be used for imaging  $\text{Hg}^{2+}$  in living cells.

In order to verify whether **RQS** possesses mitochondrial localization properties, commercial targeting reagents Mito-Tracker Green (Mito) and Lyso-Tracker Green (Lyso) were utilized to study the localization characteristics of **RQS**. As expected, highlighted yellow pixels on overlapping images were observed in Fig. 5a, and a high overlap coefficient (0.93) and Pearson's coefficient (0.93) could be calculated from the intensity correlation plot, suggesting that **RQS** was mainly distributed in the mitochondria. In contrast, red fluorescence signals of **RQS** and green fluorescence signals of Lyso were distinctly distributed in different regions, and a low overlap coefficient (0.43) and Pearson's coefficient (0.44) were observed in Fig. 5b. Co-localization experiments confirmed that **RQS** can be used as an effective mitochondrion-targeting probe for imaging  $\text{Hg}^{2+}$  in living cells. Taken together, considering a series of excellent spectral properties and mitochondrial localization properties, **RQS** can potentially be used to explore the mechanism of mitochondrial toxicity of  $\text{Hg}^{2+}$  in the next research work. In the case of scarcity of NIR probes with large Stokes shifts for monitoring  $\text{Hg}^{2+}$  in mitochondria, this work is of great importance.

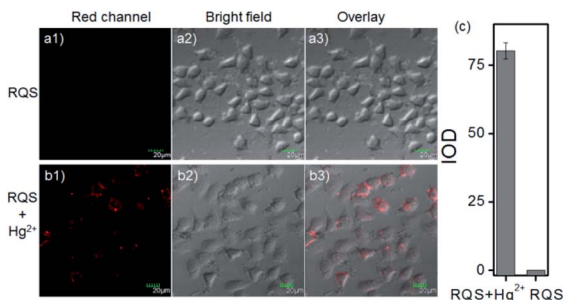


Fig. 4 Fluorescence images of HeLa cells (a1–a3) incubated with **RQS** (0.1  $\mu\text{M}$ ) for 30 min and (b1–b3) further incubated with  $\text{Hg}^{2+}$  (0.5  $\mu\text{M}$ ) for 30 min. (c) Histogram of fluorescence enhancement.  $\lambda_{\text{ex}} = 559 \text{ nm}$  and  $\lambda_{\text{em}} = 613\text{--}713 \text{ nm}$ .

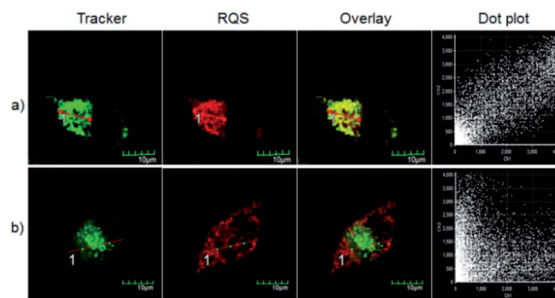


Fig. 5 Fluorescence imaging of  $\text{Hg}^{2+}$ -pretreated HeLa cells costained with **RQS** (0.1  $\mu\text{M}$ ) and other organelle-targeting trackers (200 nM): (a) costained with Mito-Tracker Green and (b) costained with Lyso-Tracker Green. Red channel:  $\lambda_{\text{ex}} = 559 \text{ nm}$ ,  $\lambda_{\text{em}} = 618\text{--}718 \text{ nm}$ ; green channel:  $\lambda_{\text{ex}} = 488 \text{ nm}$ ,  $\lambda_{\text{em}} = 520\text{--}541 \text{ nm}$ .

## Conclusions

In summary, we reported a novel mitochondrion-targeted NIR probe, **RQS**, with a large Stokes shift by tuning the D–A–D character of the rhodamine framework. As expected, **RQS** can be used for the specific detection of  $\text{Hg}^{2+}$  with multiple excellent properties such as high selectivity, high sensitivity, and a detection limit down to the nanomolar range (2 nM). Importantly, **RQS** showed specific distribution in mitochondrial regions, and it can potentially be utilized to explore the mechanism of mitochondrial toxicity of  $\text{Hg}^{2+}$  in the next research work.

## Experimental

### Instruments and reagents

All reagents and organic solvents were commercially available and of analytical grade, and were used directly without further purification unless otherwise stated. Compound structures were characterized by NMR and HRMS spectrometry.  $^1\text{H}$  NMR (400 MHz) and  $^{13}\text{C}$  NMR (100 MHz) spectra were recorded using a Bruker spectrometer with tetramethylsilane (TMS) as an internal standard. An Agilent 6510 Q-TOF LC/MS instrument (Agilent Technologies, Palo Alto, CA) was used to measure the molecular mass. A F-4600 fluorescence spectrophotometer (Hitachi Japan) and a UV-2550 UV/Vis spectrophotometer (Hitachi Japan) were used to study the spectroscopic properties. The pH was measured using a FE 20/EL 20 pH meter (Mettler-Toledo Instruments (Shanghai) Co., Ltd.). Fluorescence imaging was carried out using an Olympus FV 1000-IX81 confocal laser scanning microscope.

### Synthetic procedures

**Synthesis 1 and 2.** In this work, 4-methoxy-1,2-phenylenediamine (**1**) and 1,4-diethyl-6-methoxy-1,2,3,4-tetrahydroquinoxaline (**2**) were synthesized according to the method reported in the literature.<sup>12,18</sup>

**Synthesis of RQ.** First, 2-(4-diethylamino-2-hydroxybenzoyl) benzoic acid (688.6 mg, 2.2 mmol) and **2** (440 mg, 2 mmol) were stirred in methanesulfonic acid (6 mL) at 80  $^{\circ}\text{C}$  overnight. After cooling to room temperature, the mixture was extracted



with DCM (50 mL  $\times$  3), and the collected organic layers were dried over anhydrous NaSO<sub>4</sub>. After removing solvents, the crude product was purified by column chromatography (DCM/MeOH = 15 : 1 to 6 : 1) to afford compound **RQ** as a blue solid (736 mg, 76%). <sup>1</sup>H NMR (400 MHz, CDCl<sub>3</sub>)  $\delta$  8.13 (d,  $J$  = 6.9 Hz, 1H), 7.53 (p,  $J$  = 7.1 Hz, 2H), 7.13 (d,  $J$  = 6.8 Hz, 1H), 6.81 (d,  $J$  = 9.0 Hz, 1H), 6.51–6.46 (m, 3H), 5.86 (s, 1H), 3.52–3.43 (m, 4H), 3.40 (dd,  $J$  = 14.1, 7.0 Hz, 4H), 3.17 (dd,  $J$  = 8.4, 4.4 Hz, 2H), 3.02 (td,  $J$  = 14.1, 7.0 Hz, 1H), 2.92 (td,  $J$  = 14.2, 7.1 Hz, 1H), 1.23 (t,  $J$  = 7.1 Hz, 3H), 1.18 (t,  $J$  = 7.1 Hz, 6H), 0.86 (t,  $J$  = 7.0 Hz, 3H). <sup>13</sup>C NMR (100 MHz, CDCl<sub>3</sub>)  $\delta$  165.63, 155.98, 154.65, 153.41, 153.22, 148.15, 135.06, 134.51, 132.99, 131.14, 130.30, 130.13, 130.01, 129.54, 115.38, 113.39, 113.19, 102.42, 96.05, 94.75, 54.22, 52.50, 48.31, 47.68, 45.59, 15.52, 44.04, 12.57, 11.12, 9.16. HRMS  $m/z$  = 484.2600 calcd for C<sub>30</sub>H<sub>34</sub>N<sub>3</sub>O<sub>3</sub><sup>+</sup> [M]<sup>+</sup>, found: 484.2599.

**Synthesis of RQS.** Under stirring at room temperature, oxalyl chloride (381 mg, 3 mmol) was added dropwise to the dichloromethane (10 mL) solution of **RQ** (484 mg, 1 mmol). After being stirred for 4 h, the reaction mixture was concentrated under vacuum to give acid chloride. Then, 3 mL of saturated Na<sub>2</sub>S aqueous solution (25 mmol) was added to the crude acid chloride and the mixture was stirred for 10 h at room temperature. The mixture was extracted with EtOAc (50 mL  $\times$  3) and the collected organic layers were dried over anhydrous NaSO<sub>4</sub>. After removing solvents, the crude product was purified by column chromatography (DCM/petroleum ether = 1 : 1 to 2 : 1) to afford compound **RQS** as a pale yellow solid (309 mg, 62%). <sup>1</sup>H NMR (400 MHz, CDCl<sub>3</sub>)  $\delta$  7.85 (d,  $J$  = 7.6 Hz, 1H), 7.51 (t,  $J$  = 7.4 Hz, 1H), 7.43 (t,  $J$  = 7.4 Hz, 1H), 7.22 (d,  $J$  = 7.7 Hz, 1H), 6.72 (d,  $J$  = 8.4 Hz, 1H), 6.33–6.23 (m, 3H), 5.89 (s, 1H), 3.35–3.30 (m, 8H), 3.15 (s, 2H), 3.03–2.91 (m, 2H), 1.21–1.13 (m, 9H), 0.84 (t,  $J$  = 6.9 Hz, 3H). <sup>13</sup>C NMR (100 MHz, CDCl<sub>3</sub>)  $\delta$  198.18, 158.31, 152.48, 148.30, 144.52, 136.96, 135.47, 134.16, 131.43, 130.01, 128.05, 127.35, 122.44, 109.75, 108.15, 108.15, 107.97, 97.45, 97.10, 63.81, 46.79, 45.82, 45.42, 44.38, 12.70, 12.66, 10.41, 10.37, 9.48, 9.45. HRMS  $m/z$  = 500.2372 calcd for C<sub>30</sub>H<sub>34</sub>N<sub>3</sub>O<sub>2</sub>S<sup>+</sup> [M + H]<sup>+</sup>, found: 500.2399.

### Cell culture and fluorescence imaging

The HeLa cell line (human cervical cancer cells) was obtained from Beijing Dingguo Changsheng Biotechnology Co. Ltd. Reagents and media for the experiments were purchased from Sigma-Aldrich Chemical Company and the Beyotime Institute of Biotechnology. HeLa cells for imaging were cultured in a DMEM medium supplemented with 10% (v/v) fetal bovine serum and penicillin/streptomycin (100  $\mu$ g mL<sup>-1</sup>) in an atmosphere of 5% CO<sub>2</sub> at 37 °C. The cells were seeded at a density of 1  $\times$  10<sup>6</sup> cells per mL for imaging on 24-well plates and allowed to adhere for 12 h. HeLa cells were incubated with **RQ** (1  $\mu$ M) for 30 minutes and with **RQS** (0.1  $\mu$ M) for 30 minutes, and then Hg<sup>2+</sup> (0.5  $\mu$ M) was added and incubated for another 30 minutes. For co-localization experiments, **RQ** (100 nM) was incubated with 200 nM trackers (Mito-Tracker Green (Mito), Golgi-Tracker Green (Golgi), ER-Tracker Green (ER), and Lyso-Tracker Green (Lyso)) for 30 minutes, respectively; **RQS** (100 nM) were incubated with 200 nM trackers (Mito and Lyso) for 30 minutes,

respectively, and then treated with Hg<sup>2+</sup> (500 nM) for another 30 min. Fluorescence imaging was performed after washing the medium three times with PBS.

### Conflicts of interest

There are no conflicts to declare.

### Acknowledgements

This work was sponsored by the Natural Science Foundation of China (NNSFC 21907075; 21272172), and the Natural Science Foundation of Tianjin City (19JCZDJC32400; 18JCQNJC75900).

### Notes and references

- (a) Q. Sun, B. Aguila, J. Perman, L. D. Earl, C. W. Abney, Y. Cheng, H. Wei, N. Nguyen, L. Wojtas and S. Ma, *J. Am. Chem. Soc.*, 2017, **139**, 2786; (b) D. Banerjee, D. Kim, M. J. Schweiger, A. A. Kruger and P. K. Thallapally, *Chem. Soc. Rev.*, 2016, **45**, 2724; (c) H. N. Kim, W. X. Ren, J. S. Kim and J. Yoon, *Chem. Soc. Rev.*, 2012, **41**, 3210.
- (a) A. Renzoni, F. Zino and E. Franchi, *Environ. Res.*, 1998, **77**, 68; (b) D. W. Boening, *Chemosphere*, 2000, **40**, 1335.
- (a) A. C. Santos, S. A. Uyemura, N. A. G. Santos, F. E. Mingatto and C. Curti, *Mol. Cell. Biochem.*, 1997, **177**, 53; (b) J. M. Weinberg, P. G. Harding and H. D. Humes, *J. Biol. Chem.*, 1982, **257**, 60.
- (a) H. H. Harris, I. J. Pickering and G. N. George, *Science*, 2003, **301**, 1203; (b) N. Huang, L. Zhai, H. Xu and D. Jiang, *J. Am. Chem. Soc.*, 2017, **139**, 2428; (c) T. W. Clarkson, L. Magos and G. J. N. Myers, *N. Engl. J. Med.*, 2003, **349**, 1731.
- (a) M. Königsberg, N. E. López-Díazguerrero, L. Bucio and M. C. Gutierrez-Ruiz, *J. Appl. Toxicol.*, 2001, **21**, 323; (b) E. A. Belyaeva, D. Dymkowska, M. R. Wieckowski and L. Wojtczak, *Toxicol. Appl. Pharmacol.*, 2008, **231**, 34; (c) J. H. Southard and P. Nitisewojo, *Biochem. Biophys. Res. Commun.*, 1973, **52**, 921; (d) J. R. Brawer, G. F. McCarthy, M. Gornitsky, D. Frankel, K. Mehindate and H. M. Schipper, *Neurotoxicology*, 1998, **19**, 767.
- (a) J. Du, M. Hu, J. Fan and X. Peng, *Chem. Soc. Rev.*, 2012, **41**, 4511; (b) X. Li, X. Gao, W. Shi and H. Ma, *Chem. Rev.*, 2013, **114**, 590; (c) K. P. Carter, A. M. Young and A. E. Palmer, *Chem. Rev.*, 2014, **114**, 4564; (d) M. Taki, K. Akaoka, S. Iyoshi and Y. Yamamoto, *Inorg. Chem.*, 2012, **51**, 13075; (e) J. Chen, W. Liu, B. Zhou, G. Niu, H. Zhang, J. Wu, Y. Wang, W. Ju and P. Wang, *J. Org. Chem.*, 2013, **78**, 6121; (f) H. Agarwalla, P. S. Mahajan, D. Sahu, N. Taye, B. Ganguly, S. B. Mhaske, S. Chattopadhyay and A. Das, *Inorg. Chem.*, 2016, **55**, 12052.
- (a) Y. Sun, J. Liu, X. Lv, Y. Liu, Y. Zhao and W. Guo, *Angew. Chem., Int. Ed.*, 2012, **51**, 7634; (b) L. Yuan, W. Lin, K. Zheng, L. He and W. Huang, *Chem. Soc. Rev.*, 2013, **42**, 622; (c) J. Zhou and H. Ma, *Chem. Sci.*, 2016, **7**, 6309; (d) B. Biswal, D. Mallick and B. Bag, *Org. Biomol. Chem.*, 2016, **14**, 2241; (e) M. Zhang, X. Liu, Y. Bao and B. Yang, *Tetrahedron*, 2016, **72**, 328; (f) C. Liu, X. Jiao, Q. Wang,



- K. Huang, S. He, L. Zhao and X. Zeng, *Chem. Commun.*, 2017, **53**, 10727; (g) W. Piao, K. Hanaoka, T. Fujisawa, S. Takeuchi, T. Komatsu, T. Ueno, T. Terai, T. Tahara, T. Nagano and Y. Urano, *J. Am. Chem. Soc.*, 2017, **139**, 13713; (h) M. Deng, D. Gong, S. Han, X. Zhu, A. Lqbal, W. Liu, W. Qin and H. Guo, *Sens. Actuators, B*, 2017, **243**, 195; (i) P. E. Hande, A. B. Samui and P. S. Kulkarni, *Sens. Actuators, B*, 2017, **246**, 597.
- 8 (a) W. Duan, Y. Han, Q. Liu, J. Cui, S. Gong, Y. Ma, C. Zhang and Z. Sun, *Tetrahedron Lett.*, 2017, **58**, 271; (b) J. Tao, X. Wang, X. Chen, T. Li, Q. Diao, H. Yu and T. Wang, *Dyes Pigm.*, 2017, **137**, 601.
- 9 (a) Z. Q. Guo, S. Park, J. Yoon and I. Shin, *Chem. Soc. Rev.*, 2014, **43**, 16; (b) R. Weissleder and V. Ntziachristos, *Nat. Med.*, 2003, **9**, 123.
- 10 (a) H. Zhu, J. Fan, B. Wang and X. Peng, *Chem. Soc. Rev.*, 2015, **44**, 4337; (b) B. Kaur, N. Kaur and S. Kumar, *Coord. Chem. Rev.*, 2018, **358**, 13.
- 11 T. Ren, W. Xu, W. Zhang, X. Zhang, Z. Wang, Z. Xiang, L. Yuan and X. Zhang, *J. Am. Chem. Soc.*, 2018, **140**, 7716.
- 12 Z. Tian, B. Tian and J. Zhang, *Dyes Pigm.*, 2013, **99**, 1132.
- 13 (a) J. Qin, H. Yao, S. He and X. Zeng, *RSC Adv.*, 2016, **6**, 75570; (b) X. Jiao, C. Liu, K. Huang, S. Zhang, S. He, L. Zhao and X. Zeng, *Org. Biomol. Chem.*, 2015, **13**, 6647; (c) P. Verwilt, J. Han, J. Lee, S. Mun, H. G. Kang and J. S. Kim, *Biomaterials*, 2017, **115**, 104; (d) K. Huang, S. He and X. Zeng, *Tetrahedron Lett.*, 2017, **58**, 2004.
- 14 Y. K. Kim, H. H. Ha, J. S. Lee, X. Bi, Y. H. Ahn, S. Hajar, J. J. Lee and Y. T. Chang, *J. Am. Chem. Soc.*, 2010, **132**, 576.
- 15 (a) W. Shi and H. Ma, *Chem. Commun.*, 2008, **16**, 1856; (b) J. Liu, D. Wu, X. Yan and Y. Guan, *Talanta*, 2013, **116**, 563; (c) X. Zhan, Z. Qian, H. Zheng, B. Su, Z. Lan and J. Xu, *Chem. Commun.*, 2008, **16**, 1859; (d) X. Q. Chen, S. W. Nam, M. J. Jou, Y. Kim, S. J. Kim, S. Park and J. Y. Yoon, *Org. Lett.*, 2008, **10**, 5235; (e) L. Cui, W. Shi, J. Wang, Y. Song, H. Ma and L. Jiang, *Anal. Methods*, 2010, **2**, 448.
- 16 F. Vollmer, W. Rettig and E. Birckner, *J. Fluoresc.*, 1994, **4**, 65.
- 17 *Mercury Update: Impact of Fish Advisories*, EPA Fact Sheet EPA-823-F-01-011, EPA, Office of Water, Washington, DC, 2001.
- 18 A. R. Jagtap, V. S. Satam, R. N. Rajule and V. R. Kanetkar, *Dyes Pigm.*, 2009, **82**, 84.

